ACS Photonics

Letter

pubs.acs.org/journal/apchd5

Generation and Spatial Control of Hybrid Tamm Plasmon/Surface Plasmon Modes

Stefano Azzini,[†] Guillaume Lheureux,[†] Clementine Symonds,[*,†] Jean-Michel Benoit,[†] Pascale Senellart,[‡] Aristide Lemaitre,[‡] Jean-Jacques Greffet,[§] Cedric Blanchard,[§] Christophe Sauvan,[§] and Joel Bellessa[†]

[†]Univ Lyon, Université Claude Bernard Lyon 1, CNRS, Institut Lumière Matière, F-69622 Villeurbanne, France

[‡]Centre de Nanosciences et Nanotechnologies, CNRS Université Paris-Saclay, Route de Nozay, F-91460 Marcoussis, France

[§]Laboratoire Charles Fabry, Institut d'Optique, CNRS, Université Paris-Sud, 2 Avenue Fresnel, 91127 Palaiseau Cedex, France

Supporting Information

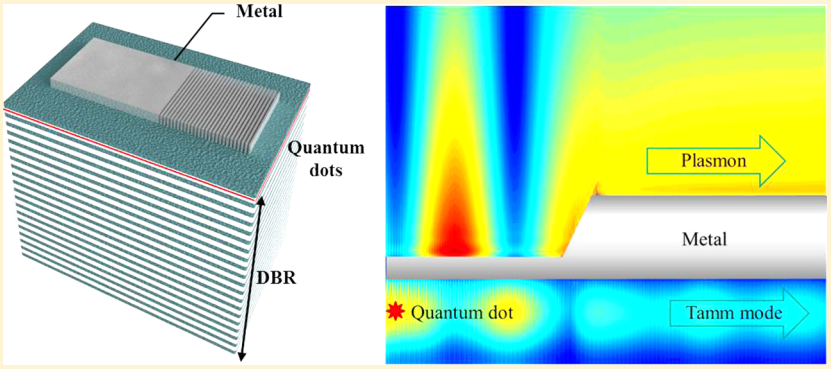

ABSTRACT: In this Letter we experimentally demonstrate the coupling between Tamm plasmon and surface plasmon modes in a metal/semiconductor integrated microstructure. The Tamm plasmon mode is excited by the photoluminescence of quantum dots grown in the top part of a dielectric Bragg mirror covered by a silver layer. The hybrid nature of such a Tamm plasmon/surface plasmon mode is demonstrated by the observation of a spatial beating along the propagation. Experimental results are in very good agreement with numerical calculations. We show how such a structure can be used and further optimized to create surface plasmons through electrical pumping. These results pave the way to a new generation of hybrid metal/semiconductor integrated optical devices for both energy-sensitive surface detection and electrical excitation of surface plasmons.

KEYWORDS: *surface plasmon, Tamm plasmon, quantum dot sources, mode beating*

Since they offer an extremely strong light confinement, surface plasmons (SPs) are widely used for sensing but also for subwavelength photonic devices.[1,2] However, integration of active light sources directly into plasmonic devices remains a challenge.[3] Coupling plasmonic structures to well-established semiconductor light sources may appear as an alternative to achieve surface plasmon generation, eventually compatible with electrical injection.[4−8] One promising approach is to couple an emitter to a SP mode via a guided mode.[9,10] Another emerging promising solution is represented by Tamm plasmon (TP) structures.[11,12] TP modes appear at the interface between a distributed Bragg reflector (DBR) and a metallic film.[11] TPs have been proven to be useful for the development of diodes and lasers.[13−15] The hybrid metal/dielectric nature of Tamm structures as well as their compatibility with semiconductor technology makes them ideal for SP generation.[16−18] Indeed, thanks to their metal part, a simple and efficient coupling geometry between the semiconductor emission and the SP at the metal/air interface can be realized. In this paper we demonstrate that emitters located in the structure can be coupled to SP modes via TP modes. Due to the deeper TP mode extension into the semiconductor compared to SP modes, this conversion can be efficient even if the emitters are buried far from the metallic film. We also demonstrate that this coupling leads to a spatial beating along the propagation direction, yielding a spatial control of the quantum dot emission/SP coupling.

In order to illustrate the TP/SP coupling, the dispersion relation of a typical TP structure (Figure 1a) calculated by the transfer-matrix method is displayed in Figure 1b. The calculated passive structure consists of a 33 nm thick planar silver film on top of a 65-pair DBR, with no emitters embedded in the DBR. The TP mode is characterized by a narrow-line-width (∼1 nm) parabolic dispersion. This reduced line width compared to SP is related to the TP field distribution lying mainly in the semiconductor part of the structure:[11] the field presents decaying oscillations in the DBR on typically 0.6 μm and a fast decay in the metal over ∼15 nm. The quasi-vertical lines

Received: July 22, 2016
Published: September 19, 2016

DOI: 10.1021/acsphotonics.6b00521
ACS Photonics 2016, 3, 1776−1781

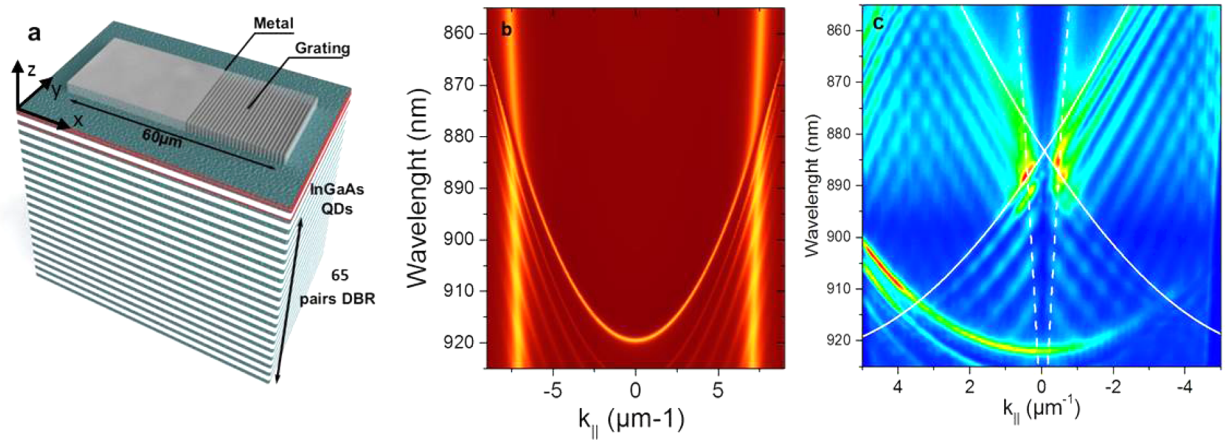

Figure 1. (a) Sketch of the structure. The active region of the DBR is formed by three InAs QD monolayers embedded in the two uppermost GaAs $\lambda/4$ layers. The 33 nm thick silver film deposited on top consists of a 30 × 30 μm flat area next to a 30 × 30 μm outcoupling area (grating period 0.9 μm, filling factor 0.55). (b) Dispersion relation of the structure calculated by the transfer-matrix method. The bright lines lying slightly outside the light cone ($k_{||} \approx 7\ \mu m^{-1}$) correspond to the silver/air SP, the brighter parabola corresponds to the TP, and the parabola lying at longer wavelengths corresponds to the Bragg modes of the structure. An anticrossing is visible in the region where SP and TP should cross. (c) Experimental dispersion relations with excitation and detection on the grating area. The solid (respectively dashed) white lines correspond to the folding (+1 and −1 diffracted orders) of the calculated Tamm mode (respectively surface plasmon mode).

are attributed to the SP mode at the metal/air interface. Below the TP dispersion line, several parabolic lines corresponding to the higher order modes of the DBR are present (Bragg modes). An anticrossing between the SP and TP modes takes place as a consequence of their optical coupling inside the metallic layer. The coupling strength is mainly sensitive to the metal thickness.[16,18] TP and SP modes always match in energy and wavevector under the light cone, so that their optical coupling occurs for in-plane propagation. A grating is thus necessary for light outcoupling and detection. This grating will be used both for direct measurement of dispersion relations (Figure 1c) and for light extraction after propagation along an unpatterned area (Figure 1a).

Our Tamm structure DBR is formed by a 65-pair stack of $GaAs/Al_{0.95}Ga_{0.05}As$ $\lambda/4$ layers grown on a GaAs substrate by molecular beam epitaxy. Three pairs of highly dense self-assembled InAs/GaAs quantum dot (QD) layers are embedded in the two upper GaAs layers of the dielectric stack. The Tamm structure metallic part is defined by e-beam lithography, using a PMMA resist, forming 30 μm × 60 μm rectangles. A 33 nm thick silver layer is then deposited by thermal evaporation. As shown in Figure 1a, the silver rectangles are formed by a 30 μm × 30 μm unpatterned area next to a 30 μm × 30 μm 1D grating (period ∼900 nm, metal filling factor ∼0.55), referred to as the outcoupling area in the following. No lift-off of the PMMA is performed after the metal deposition, in order to prevent QD emission collection from outside the structure of interest. Photoluminescence (PL) experiments are performed at 77 K. The devices are excited from the top with a continuous-wave Ti:sapphire laser at 760 nm, focused on the sample to form a ∼1.8 μm diameter spot using a microscope objective (numerical aperture (NA) = 0.75). The emitted light is collected by the same objective and sent to a spectrometer equipped with a silicon CCD array. To measure the radiation patterns, the microscope objective Fourier plane is imaged on the spectrometer entrance slits. In order to evaluate properly the surface plasmon contribution, only the TM polarization of the emission is selected.

Figure 1c shows a PL intensity colored map as a function of the wavelength and the in-plane wavevector, obtained for optical excitation within the grating area. The dispersion relations of all the optical modes supported by the structure are folded inside the light cone due to the presence of the grating. Indeed, in addition to the zero-order TP mode centered at ∼920 nm (together with the other zero-order Bragg modes visible at longer wavelengths), the presence of folded TP and SP modes can be clearly observed. In particular, the folded first-order TPs and SPs can be easily identified (highlighted in Figure 1c with solid and dashed white lines, respectively). The bright region in Figure 1c between 870 and 890 nm around $k_{<} = 0$, where the highlighted modes cross each other, corresponds to TP/SP optical coupling within the light cone. Because of the large number of folded lines (TP, SP, Bragg modes) it is however difficult to evidence directly an anticrossing behavior between the TP and SP modes. Additional losses for the TP and SP modes generated by the grating could also explain the difficult observation of the anticrossing in the grating region. It can also be noted that the emission mainly comes from the TP, the emission in the SP branch being weak far from the interaction region. This is an indication that the major part of the QDs' emission is directed through the TP mode.

To investigate the TP/SP mode propagation, the sample is now excited far away from the grating in the flat silver region (Figure 2a). The emission along a vertical section is recorded by imaging the sample surface on the spectrometer entrance slit. A spectral image is displayed in Figure 2b: the horizontal axis corresponds to the wavelength and the vertical axis to the vertical position along the propagation direction. The zero position corresponds to the grating interface. The intense amount of light originating from the −26 μm position results from the emission at the excitation spot position, and the weaker spots around the 0 μm position from the light outcoupled by the grating. No light is collected between these two positions, along the propagation path, indicating that the emission at the grating interface emanates from the propagation of modes lying below the light cone. To identify more clearly the origin of this emission, we selected the spatial region around the grating interface in an intermediate image plane and performed Fourier-space imaging. The result, which characterizes spectrally and angularly only the modes remaining

DOI: 10.1021/acsphotonics.6b00521
ACS Photonics 2016, 3, 1776−1781

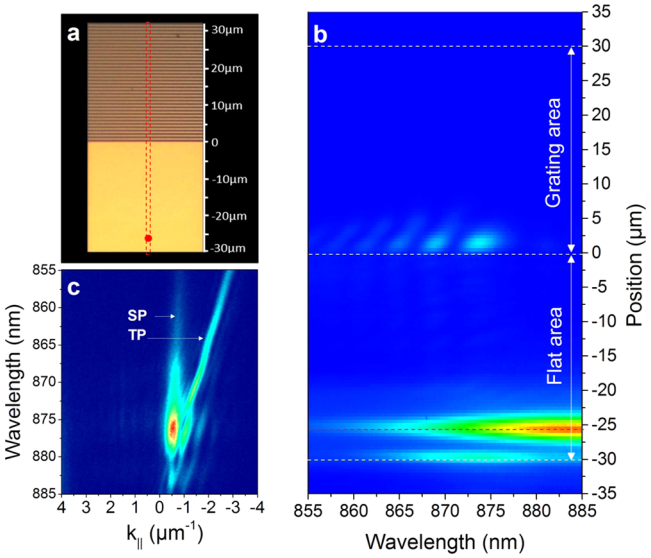

Figure 2. (a) Microscopy image of the sample surface. The red dot corresponds to the excitation region. The dashed red lines show the vertical cross section selected by the spectrometer entrance slit. (b) Wavelength-resolved image of the emission along the sample vertical direction. The horizontal dashed white lines mark the borders of the flat and patterned areas; the horizontal dashed red line corresponds to the excitation spot position. (c) Fourier image of the emission collected at the grating interface, obtained by selecting this region in an intermediate image plane. The white arrows indicate the Tamm plasmon (TP) and surface plasmon (SP) modes.

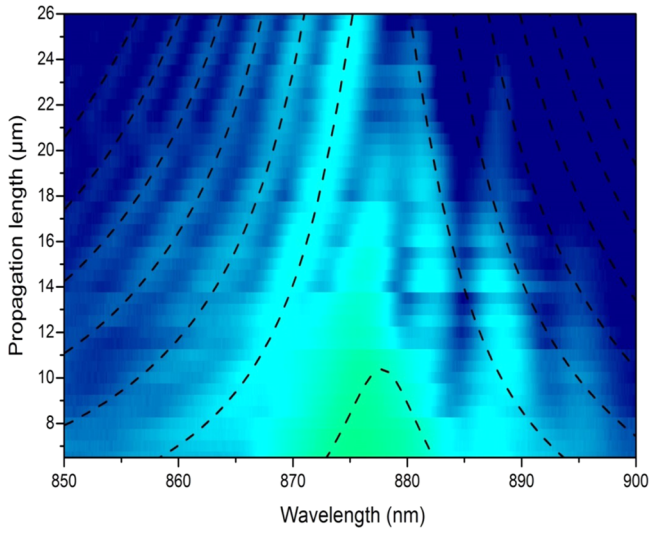

Figure 3. Spectral distribution of the intensity (in log scale) recorded at the grating interface as a function of the excitation spot distance. Each horizontal line has been obtained by selecting the emission at the grating interface for the corresponding distance. The black dashed lines are the calculated distances corresponding to $(m + 1/2)$ oscillations between the TP/SP coupled modes (m = 0 to 6).

after propagation over 26 μm, is shown in Figure 2c. This Fourier space image indicates that between 875 and 880 nm the emission detected at the grating interface can be associated with a TP/SP coupled mode. It has to be noticed that the signal that comes from the outcoupling of the SP is here brighter than the one associated with the TP, contrary to the measurement performed directly in the grating area (Figure 1c).

One striking feature of the light outcoupled by the grating is the observation of a pattern in the broad emission spectrum, which appears in Figure 2b. When the vertical position of the excitation spot, and thus the propagation length before extraction by the grating, is modified, a substantial wavelength shift of the spectral pattern occurs. These wavelength maxima measured at the grating interface as a function of the excitation distance are summarized in Figure 3. This figure shows that the intensity oscillates with the propagation length, with a period depending on the wavelength. This behavior can be explained by a spatial beating between the coupled TP/SP modes. A physical picture of the beating, which will be more quantitatively described in the next section, can be obtained by considering a simple coupled oscillator model, where the TP mode and the SP mode interact via a coupling constant g. For a given wavelength, a wave-vector difference Δk can be defined between the TP/SP coupled modes. The spatial beating is directly related to Δk, which itself depends on the wavelength. This spatial beating corresponds to an oscillation of the energy between the air region, which can be associated with a bare plasmon mode (plasmon-like mode), and the semiconductor region associated with the bare Tamm mode (Tamm-like mode). The coupled modes are a superposition of these Tamm-like and plasmon-like modes. As the QDs are located in the semiconductor part, they couple to a superposition of hybrid modes that propagate with different wavevectors. During the propagation the phase between both modes changes, leading to the beating between the air and semiconductor region. As we can assume that the QD layer emission mainly excites the Tamm-like mode and that the metallic grating is more sensitive to the plasmon-like mode, light will be extracted only if $(m + 1/2)$ oscillations have occurred along the propagation. This has been modeled using the dispersion relations of TP and SP and a coupling constant g = 9 meV. We calculated the propagation distance corresponding to $(m + 1/2)$ oscillations with $L = \frac{2\pi}{\Delta k}(m + 1/2)$ where m is the number of oscillations. The results are plotted in dashed lines in Figure 3 for m = 0 to m = 6. For wavelengths below the resonance (around 878 nm), our calculations are in excellent agreement with the experiments. At higher wavelengths, the oscillation presents a more complex behavior that cannot be fitted with this simple model. This is due to the presence of the Bragg modes, as will be shown in the next section.

To take into account the system complex modal structure, numerical simulations have been carried out. Figure 4a presents the dispersion relations corresponding to the Tamm plasmon, the silver/air surface plasmon, and the first four Bragg modes. The dispersion relations of the unpatterned planar structure have been calculated with the scattering-matrix method by looking for poles of the total scattering matrix with a real frequency and a complex wave vector. The calculations evidence the anticrossing between the TP and the SP modes, indicating a coupling between these two modes. For a wavelength slightly below resonance (878 nm) the electric field profile of both coupled modes shows their hybrid nature, with oscillations in the DBR and an exponential decay in the air (Figure 4c). Farther from the anticrossing (840 nm), the modes present a more plasmon-like (electric field mainly in the air) and Tamm-like (electric field mainly in the DBR) behavior, as shown in Figure 4b and d, respectively. It can also be seen in the dispersion relations that the SP mode interacts not only with the TP mode but also with the Bragg modes lying at longer wavelength. This explains why above 880 nm the

DOI: 10.1021/acsphotonics.6b00521
ACS Photonics 2016, 3, 1776−1781

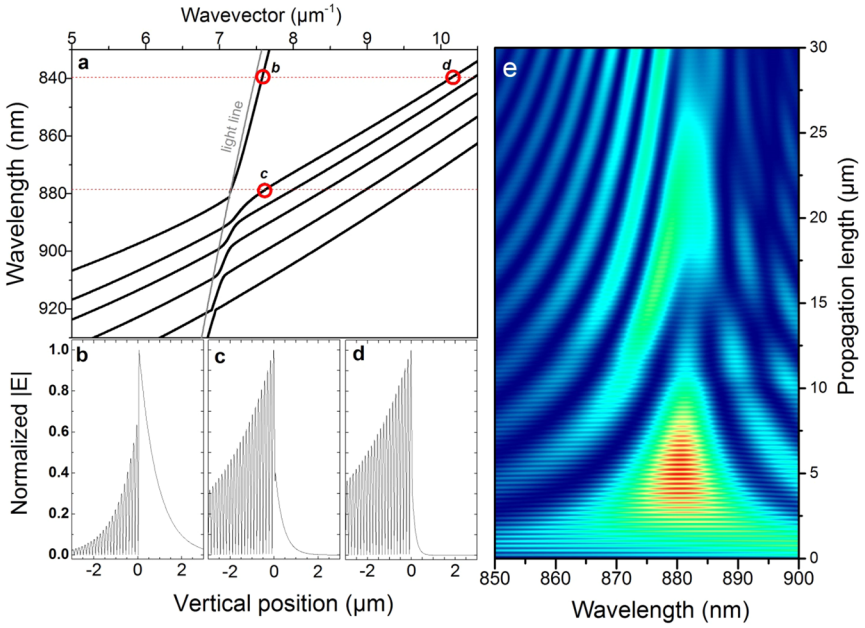

Figure 4. Numerical simulations. (a) Dispersion relations of the modes of the unpatterned structure with a 33-nm-thick silver film structure. The red circles indicate the positions in the dispersion relations where the modulus of the longitudinal component of the electric field has been calculated: (b) and (d) at 840 nm; (c) at 878 nm. (e) Spectral distribution of the intensity in air of the light emitted in the unpatterned structure as a function of the horizontal distance to the source.

oscillating behavior cannot be accurately described by the beating of only two modes. This effect is further evidenced when calculating the intensity in air of the light emitted in the unpatterned area as a function of the propagation length and the wavelength, presented in Figure 4e. For the calculation, the QD emission has been modeled by a line current source with an in-plane polarization, $\mathbf{j} = j_0\delta(x, z - z_0)\mathbf{u}_x$, with x (respectively z) being the direction parallel (respectively perpendicular) to the stack. The source is located in the first GaAs layer, at $x = 0$ and $z_0 = -42$ nm below the metal/semiconductor interface. The electromagnetic field in this planar system in TM polarization has been analytically calculated as an integral over the wave vector component parallel to the interfaces of the stack. Since the intensity of the light outcoupled by the grating is proportional to the intensity incident on the grating, the results of the calculation can be directly compared to the experimental results presented in Figure 3. The oscillating behavior at wavelengths below 880 nm (i.e., for energies above resonance) is well reproduced by the calculations as well as the complex modulation above 880 nm (i.e., for energies below resonance). Note that the calculations also clearly show high-frequency oscillations superimposed on the beating between the two hybrid TP/SP modes. These oscillations can unambiguously be attributed to an additional beating with the SP supported by the metal/semiconductor interface (see Supporting Information). Since the propagation length of this SP is much smaller than that of the two hybrid modes, the fast oscillations almost completely disappear after propagation over 20 μm; see Figure 4e.

The electric field distribution in the (x, z) plane at a fixed wavelength of 878 nm in the unpatterned structure is presented in Figure 5a, where the vertical axis (z) corresponds to the growth direction and the horizontal axis (x) to the propagation distance, parallel to the layer plane. The source is located at $x = 0$ and the map starts at $x = 15$ μm. Along the propagation, the intensity profile evidences the alternative Tamm-like and plasmon-like behavior of the coupled modes: for the plasmon-like mode a large part of the energy is located in the air, while for the Tamm-like mode almost all the energy is located in the DBR.[11] A very promising aspect of this approach for SP generation is that, as the Tamm mode electric field presents a large extension inside the DBR, one can locate the emitter far beneath the metallic layer. Indeed, when placing the source in the third GaAs layer (~300 nm below the metallic layer), the intensity distribution presents the same oscillating behavior between Tamm-like and plasmon-like modes (see Supporting Information). It is thus possible to couple the emission of deeply buried semiconductor QDs to the metal/air surface plasmon in a planar geometry. This last point is a key point for surface plasmon generation. Indeed, for electrical injection, the emitter−metal distance has to be larger than the depletion length of the carriers close to a conducting surface.[19] This condition, which cannot be fulfilled with a direct coupling to SPs (typically coupling distance of a few tens of nanometers), is released with the TP/SP coupling geometry presented here.

Up to this point, our experimental geometry has led to the formation of hybrid TP/SP modes because of the metallic layer thinness. We propose now a scheme that would enable the generation of pure SP from a TP structure. In order to progressively turn off the Tamm/plasmon coupling and obtain pure SP, we consider a structure comprising a wedge where the metal thickness increases continuously from 33 nm to 120 nm over a length of 3 μm. In that case, a hybrid mode, generated in the thin metallic region, would transform into pure TP and SP modes while propagating through the wedge. SP generation can be maximized by adjusting the emitter−wedge separation so that $(m + 1/2)$ oscillations take place. The calculated electric field distribution in this configuration is presented in Figure 5b, with a source−wedge separation of 43.8 μm optimized for SP coupling, with the source being located at $x = 0$. A wavelength close to the resonance has to be chosen to maximize the

DOI: 10.1021/acsphotonics.6b00521
ACS Photonics 2016, 3, 1776−1781

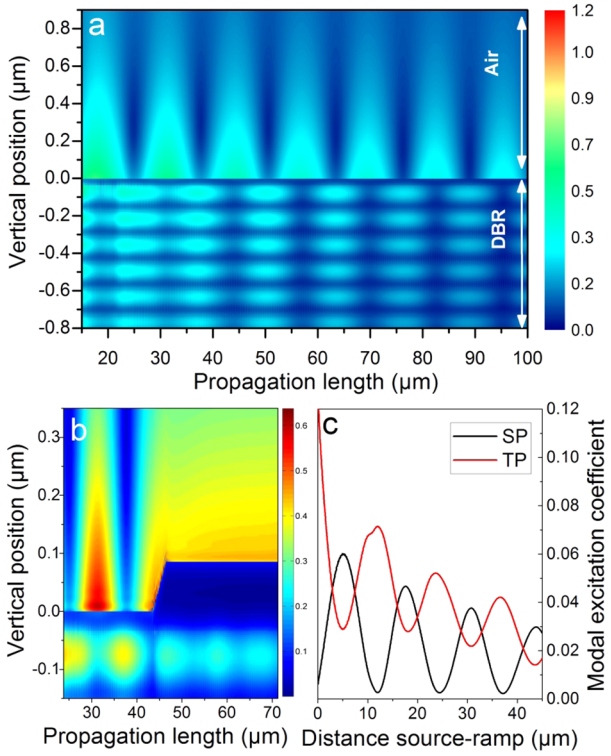

Figure 5. (a) Electric field distribution |*E*| emitted by the source at 878 nm in the planar structure with a 33-nm-thick flat silver layer. The vertical direction (z) is perpendicular to the layer planes; the horizontal axis (x) corresponds to the propagation direction. (b) Electric field distribution |*E*| emitted by the source at 878 nm in the presence of a 3-μm-long wedge; the silver thickness is progressively increased from 33 nm to 120 nm. The wedge starts at a distance of 43.8 μm from the source. In (a) and (b) the source is located at $x = 0$ and 42 nm below the metal/DBR interface. (c) Amplitudes $|A_{SP}|^2$ and $|A_{TP}|^2$ of the SP and the TP modes at the top of the metallic wedge as a function of the distance between the source and the wedge. The amplitudes have been normalized by the total power emitted by the source.

hybridization between SP and TP and thus foster the energy transfer. The calculation has been performed with the aperiodic Fourier modal method (a-FMM)[20] at a wavelength of 878 nm. Large coupling of the light to the metal/air SP is clearly visible. In the region with the 120-nm-thick silver film (wedge top position), the total electromagnetic field can be written as a sum over the modes (radiative and nonradiative) of the planar structure. By using the mode orthogonality in absorbing waveguides,[21] it is possible to extract the amplitudes A_{SP} and A_{TP} of the TP and SP modes from the total field calculated with the a-FMM. These amplitudes are shown in Figure 5c, as a function of the source−wedge separation. The results have been normalized by the total power emitted by the source. This figure shows the expected oscillations, indicating that coupling to SP or to TP modes can be controlled by adjusting the separation. A maximum coupling efficiency of 6% is obtained. The SP generation can also be modified by changing the metal thickness. A coupling of 7% could for example be obtained by choosing a silver thickness of 43 nm (see Supporting Information).

In conclusion, we demonstrate that emission of QDs inserted in a Tamm structure can be coupled to hybrid TP/SP modes. This leads to spatial beating of the field intensity between plasmon in air and TP in a semiconductor. The beating is exploited to couple the QDs' emission into a surface plasmon mode. Our approach brings together Tamm structures, efficient for lasing and diodes, with a propagating surface plasmon at the metal/air interface, which are usable for plasmonic circuits. Indeed, the transfer shown in this paper for a 2D metallic film could be applied to metallic stripes, which could also lead to a better control of the emitted light. This simple geometry is also fully compatible with electrical injection, as a close proximity between metal and emitters is not required. The coupling of plasmonic structures to well-established semiconductor devices also offers perspectives for sensing, by integrating semiconductor light detectors in plasmonic setups.

■ ASSOCIATED CONTENT

Supporting Information

The Supporting Information is available free of charge on the ACS Publications website at DOI: 10.1021/acsphotonics.6b00521.

Refractive indexes used for numerical simulation; cartography of the electric field: evidence of the interaction with the semiconductor/metal surface plasmon and impact of the emitter vertical position; variation of the SP modal excitation coefficient with the metal thickness (PDF)

■ AUTHOR INFORMATION

Corresponding Author

*E-mail: clementine.symonds@univ-lyon1.fr.

Notes

The authors declare no competing financial interest.

■ ACKNOWLEDGMENTS

The authors acknowledge Jean-Paul Hugonin for fruitful discussions and computational assistance. The authors acknowledge financial support from Agence Nationale de la Recherche (ANR) on ANR project NEHMESIS

■ REFERENCES

(1) Barnes, W. L.; Dereux, A.; Ebbesen, T. W. Surface plasmon subwavelength optics. *Nature* **2003**, *424*, 824.

(2) Lal, S.; Link, S.; Halas, N. J. Nano-optics from sensing to waveguiding. *Nat. Photonics* **2007**, *1*, 641−648.

(3) Sorger, V. J.; Oulton, R. F.; Ma, R. M.; Zhang, X. Toward integrated plasmonic circuits. *MRS Bull.* **2012**, *37*, 728−738.

(4) Babuty, A.; Bousseksou, A.; Tetienne, J. P.; Doyen, I. M.; Sirtori, C.; Beaudoin, G.; Sagnes, I.; De Wilde, Y.; Colombelli, R. Semiconductor Surface Plasmon Sources. *Phys. Rev. Lett.* **2010**, *104*, 226806.

(5) Neutens, P.; Lagae, L.; Borghs, G.; Van Dorpe, P. Electrical Excitation of Confined Surface Plasmon Polaritons in Metallic Slot Waveguides. *Nano Lett.* **2010**, *10*, 1429−1432.

(6) Fan, P.; Colombo, C.; Huang, K. C. Y.; Krogstrup, P.; Nygård, J.; Fontcuberta i Morral, A.; Brongersma, M. L. An Electrically-Driven GaAs Nanowire Surface Plasmon Source. *Nano Lett.* **2012**, *12*, 4943−4947.

(7) Li, J.; Wei, H.; Shen, H.; Wang, Z.; Zhao, Z.; Duanb, X.; Xu, H. Electrical source of surface plasmon polaritons based on hybrid Au−GaAs QW structures. *Nanoscale* **2013**, *5*, 8494.

(8) Rai, P.; Hartmann, N.; Berthelot, J.; Arocas, J.; Colas des Francs, G.; Hartschuh, A.; Bouhelier, A. Electrical Excitation of Surface Plasmons by an Individual Carbon Nanotube transistor. *Phys. Rev. Lett.* **2013**, *111*, 026804.

(9) Costantini, D.; Greusard, L.; Bousseksou, A.; Rungsawang, R.; Zhang, T. P.; Callard, S.; Decobert, J.; Lelarge, F.; Duan, G.-H.; De

DOI: 10.1021/acsphotonics.6b00521
ACS Photonics 2016, 3, 1776−1781

Wilde, Y.; Colombelli, R. In Situ Generation of Surface Plasmon Polaritons Using a Near-Infrared Laser Diode. *Nano Lett.* **2012**, *12*, 4693−4697.
(10) Fedyanin, D. Y.; Krasavin, A. V.; Arsenin, A. V.; Zayats, A. V. Surface Plasmon Polariton Amplification upon Electrical Injection in Highly Integrated Plasmonic Circuits. *Nano Lett.* **2012**, *12*, 2459−2463.
(11) Kaliteevski, M.; Iorsh, I.; Brand, S.; Abram, R. A.; Chamberlain, J. M.; Kavokin, A. V.; Shelykh, I. A. Tamm plasmon-polaritons: Possible electromagnetic states at the interface of a metal and a dielectric Bragg mirror. *Phys. Rev. B: Condens. Matter Mater. Phys.* **2007**, *76*, 165415.
(12) Sasin, M. E.; Seisyan, R. P.; Kalitteevski, M. A.; Brand, S.; Abram, R. A.; Chamberlain, J. M.; Egorov, A. Y.; Vasil'ev, A. P.; Mikhrin, V. S.; Kavokin, A. V. Tamm plasmon polaritons: Slow and spatially compact light. *Appl. Phys. Lett.* **2008**, *92*, 251112.
(13) Symonds, C.; Lheureux, G.; Hugonin, J.-P.; Greffet, J.-J.; Laverdant, J.; Brucoli, G.; Lemaître, A.; Senellart, P.; Bellessa, J. *Nano Lett.* **2013**, *13*, 3179−3184.
(14) Bruckner, R.; Zakhidov, A. A.; Scholz, R.; Sudzius, M.; Hintschich, S. I.; Frob, H.; Lyssenko, V. G.; Leo, K. Phase-locked coherent modes in a patterned metal-organic microcavity. *Nat. Photonics* **2012**, *6*, 322−326.
(15) Lheureux, G.; Azzini, S.; Symonds, C.; Senellart, P.; Lemaître, A.; Sauvan, C.; Hugonin, J.-P.; Greffet, J.-J.; Bellessa, J. *ACS Photonics* **2015**, *2*, 842−848.
(16) Afinogenov, B. I.; Bessonov, V. O.; Nikulin, A. A.; Fedyanin, A. A. *Appl. Phys. Lett.* **2013**, *103*, 061112.
(17) Lopez-Garcia, M.; Ho, Y.-L. D.; Taverne, M. P. C.; Chen, L.-F.; Murshidy, M. M.; Edwards, A. P.; Serry, M. Y.; Adawi, A. M.; Rarity, J. G.; Oulton, R. *Appl. Phys. Lett.* **2014**, *104*, 231116.
(18) Chen, Y.; Zhang, D.; Zhu, L.; Fu, Q.; Wang, R.; Wang, P.; Ming, H.; Badugub, R.; Lakowicz, J. R. Effect of metal film thickness on Tamm plasmon-coupled emission. *Phys. Chem. Chem. Phys.* **2014**, *16*, 25523.
(19) Kwon, M. K.; Kim, J. Y.; Kim, B. H.; Park, I. K.; Cho, C. Y.; Byeon, C. C.; Park, S. J. Surface-Plasmon-Enhanced Light-Emitting Diodes. *Adv. Mater.* **2008**, *20*, 1253−1257.
(20) Silberstein, E.; Lalanne, P.; Hugonin, J. P.; Cao, Q. Use of grating theories in integrated optics. *J. Opt. Soc. Am. A* **2001**, *18*, 2865−2875.
(21) Snyder, A. W.; Love, J. D. *Optical Waveguide Theory*; Chapman and Hall: New York, 1983.

DOI: 10.1021/acsphotonics.6b00521
ACS Photonics 2016, 3, 1776−1781